Resonant x-ray scattering study of charge superstructures in layered $La_{2-x}Ca_xCoO_{4\pm\delta}$ ($0.4 \leqslant x \leqslant 0.7$) and $La_{1.5}Sr_{0.5}CoO_4$ compounds

J. García,[1] G. Subías,[1,*] J. Blasco,[1] M. C. Sánchez,[1] and G. Beutier[2]

[1]*Instituto de Ciencia de Materiales de Aragón, Departamento de Física de la Materia Condensada, CSIC-Universidad de Zaragoza, C/ Pedro Cerbuna 12, 50009 Zaragoza, Spain*

[2]*Université Grenoble Alpes, Centre National de la Recherche Scientifique, Grenoble INP, SIMAP, F-38000 Grenoble, France*

(Received 4 December 2017; revised manuscript received 26 January 2018; published 7 February 2018)

We propose a model for the Co charge disproportionation in $La_{2-x}Ca_xCoO_{4\pm\delta}$ ($0.4 \leqslant x \leqslant 0.7$) and $La_{1.5}Sr_{0.5}CoO_4$ layered cobaltites based on the photon energy, azimuthal angle, and polarization dependence of the scattered intensity of selected reflections in a resonant x-ray scattering experiment. Tetragonal superlattice ($h/2$, $h/2$, l)-type reflections were detected at room temperature for all the samples independently from the Ca (or Sr) doping rate in agreement with a checkerboard ordering of two different Co sites. The corresponding average charge disproportion is accounted for by a semiempirical model from which the imaginary part of the resonant atomic scattering factors of each of the two Co atoms is obtained resulting in about 0.5 ± 0.1 electron. Moreover, no forbidden ($h/4$, $h/4$, l)-type reflections were observed at room temperature indicating the lack of any local anisotropy ordering in contrast with the behavior found in the related layered manganites. Finally, we found the pattern of small distortions ($\sim$0.05 Å) around the two Co sites compatible with the resonant x-ray scattering results. The symmetry of this displacement pattern is consistent with the $A2mm$ (or $Ammm$) orthorhombic structure of the ordered phase and the structural transition is accounted for by the condensation of two soft modes—$X_1^+(B_{2u})$ and $X_1^+(A_1)$—acting on the oxygen atoms.

DOI: 10.1103/PhysRevB.97.085111

I. INTRODUCTION

Hole-doped transition-metal oxides exhibit a large variety of intriguing phenomena, including unconventional superconductivity, metal-insulator transitions, giant magnetoresistance, and magnetoelectric behavior [1–4]. In particular, A_2BO_4 oxides with K_2NiF_4 structure (or layered perovskite) undergo structural phase transitions with decreasing temperature due to the rich interplay between charge, spin, and orbital and lattice degrees of freedom. The structure of these compounds is built up by alternate perovskite (ABO_3) and rock salt (AO) layers along the c axis. The result is a very anisotropic family of compounds where the conductivity (or electronic delocalization) within the ab plane is quite higher than perpendicular to it [5]. The undoped compounds usually are insulators and exhibit long-range antiferromagnetic ordering. At small levels of doping, hole localization leads to stripelike charge order in layered cuprates [6], in nickelates [7–9], and recently in layered cobaltites [10]. At half doping, $x = 0.5$, the transition metal has a nominal semi-integer valence and the structural transition coupled to an electronic localization is described in terms of a charge ordering (CO) transition, where the periodic ordering of the holes leads to an ordered sequence of two ionic species. If at least one of the ionic species is active to develop a Jahn-Teller effect, the CO transition may be coupled to an orbital ordering (OO) as reported for some manganites [11]. For layered perovskites, the usual pattern of CO is a checkerboard. This CO pattern has been reported in $La_{1.5}Sr_{0.5}NiO_4$ [6] and $La_{0.5}Sr_{1.5}MnO_4$ [11,12]. However, previous investigations have shown small charge difference between the two nonequivalent Mn ions in the later compound [13–15]. In fact, a recent study using high-resolution synchrotron x-ray powder diffraction and resonant x-ray scattering (RXS) in $La_{0.5}Sr_{1.5}MnO_4$ revealed that the two nonequivalent Mn sites are ordered following a checkerboard pattern but the transition is driven by the condensation of three soft modes [13]. In addition, there are systems where the checkerboard CO competes with other patterns and, for instance, the checkerboard CO of $La_{1.5}Sr_{0.5}NiO_4$ rearranges into a stripe type with decreasing temperature due to spin-charge coupling [16]. These results expose that physical mechanisms for CO in Mott-Hubbard insulators still remain unclear and more studies on related systems are needed to shed light about these complex electronic phenomena. In this way, we have chosen the layered perovskites, $La_{2-x}Ca_xCoO_{4\pm\delta}$, which are isostructural to previous systems. But cobalt oxides (or cobaltites) have the additional challenge of spin transitions. On the one hand Co^{2+} is one of the few electronic configurations in $3d$ metals where the orbital angular moment is not completely quenched and achieves significant values [17,18]. On the other hand, Co^{3+} can take different spin states. Considerable research effort has been spent on cobaltites with Co^{3+} to understand the rich phenomenology which is associated to the comparable energies of crystal-field splitting and electron-electron coupling [18–22]. This cation can exist as low spin Co^{3+} ($S = 0$, $t_{2g}{}^6e_g{}^0$), intermediate spin Co^{3+} ($S = 1$, $t_{2g}{}^5e_g{}^1$), and high spin Co^{3+} ($S = 2$, $t_{2g}{}^4e_g{}^2$).

This paper is focused on the $La_{2-x}(Sr/Ca)_xCoO_{4\pm\delta}$ system with x values close to 0.5, which shows quite peculiar transport

*Corresponding author: gloria@unizar.es

and magnetic properties [10,22–24]. These compounds adopt the tetragonal structure of layered perovskites (space group $I4/mmm$, no. 139) and Co atoms are located at the Wyckoff position $2a$. However, convergent beam electron-diffraction measurements on $La_{1.5}Ca_{0.5}CoO_4$ determined the existence of some weak reflections not accounted for by a tetragonal cell [25]. The slight deviation from tetragonal symmetry leads to an orthorhombic distortion with space group $A2mm$ (no. 35). The orthorhombic unit cell is related to the tetragonal one by the following relationships: $\mathbf{a}_o = \mathbf{a}_t + \mathbf{b}_t$, $\mathbf{b}_o = \mathbf{a}_t - \mathbf{b}_t$, and $\mathbf{c}_o = \mathbf{c}_t$, where o and t subscripts stand for orthorhombic and tetragonal cells, respectively. The tetragonal site of Co atoms is split into two nonequivalent sites in the orthorhombic cell, namely, the $2a$ (Co1) and $2b$ (Co2) Wyckoff positions.

It is well known that RXS measurements are a powerful tool for unraveling CO and OO. It has been successfully used in determining the CO nature in layered manganites [13,26–27] or related layered cobaltites with ordered oxygen vacancies [28]. A previous RXS experiment [29] on $La_{1.5}Ca_{0.5}CoO_4$ found resonant reflections indexed as $(h/2, h/2, l)_t$. The analysis was performed in the $A2mm$ orthorhombic cell and concluded a checkerboard CO pattern with a full charge disproportionation, i.e., alternating Co^{2+} and Co^{3+} cations occupying the two nonequivalent Co sites. However, the authors only studied a limited set of resonant reflections and the structure factor of them was only qualitatively described without an estimation of the Thomson scattering term. Without this term, the error in the calculation of the charge disproportionation in the Co sublattice may be large. In addition, they found that the same CO is observed for samples with $x \neq 0.5$, i.e., it does not depend on doping [25]. This result is opposite to the one observed in layered manganites where an incommensurate CO has a modulation vector that follows the doping rate [26–27].

The aim of this paper is to provide a quantitative determination of the charge disproportionation order of cobalt atoms in the doped $La_{2-x}Ca_xCoO_{4\pm\delta}$ ($x = 0.4$, 0.5, 0.6, 0.7) and $La_{1.5}Sr_{0.5}CoO_4$. This allows us to reveal the actual nature of the CO transition in this family of layered cobaltites and the origin for the observed differences with related compounds. For this purpose, we have performed RXS measurements at the Co K edge in a wider set of resonant reflections. The energy, azimuthal, and polarization dependences of these reflections have been determined. The full analysis provides us a detailed description of the electronic localization and structural distortions giving rise to the CO pattern in these layered cobaltites. Our results indicate that the two nonequivalent Co sites are arranged following the checkerboard CO pattern already found in the related layered manganites [13]. Also in this case, the charge disproportionation between both sites is smaller than one electron. However, differently from the layered manganites [13,26,27], this checkerboard CO pattern is stable for compositions $x \neq 0.5$ and no signature of any local anisotropy (so-called OO) order is found.

II. EXPERIMENTAL SECTION

Polycrystalline $La_{2-x}Ca_xCoO_{4\pm\delta}$ ($x = 0.4$, 0.5, 0.6, and 0.7) and $La_{1.5}Sr_{0.5}CoO_4$ samples were prepared by the solid-state chemistry method. Stoichiometric amounts of La_2O_3, $CaCO_3$ (or $SrCO_3$), and Co_3O_4 were mixed and heated at 960 °C in air overnight. The powders were pressed into pellets and sintered at 1300 °C in air for 24 h. This step was repeated once and the resulting samples were analyzed by x-ray diffraction showing patterns typical of a single phase. Thus, the powders were pressed into rods and sintered in the same conditions to be used for crystal growth. This growth was made in a homemade floating-zone furnace with two semielliptical mirrors [30]. The growths were carried out in dry air atmosphere with a growth speed ranging between 6 and 8 mm/h. The chemical composition of the boules was also tested using wavelength dispersive x-ray fluorescence spectrometry (Advant'XP+ model from Thermo-ARL) and the La:Sr/Ca:Co stoichiometry agreed with the expected values in all cases within the experimental error (1%). Selected parts of the boules were ground and analyzed by powder x-ray diffraction. Rietveld analysis of the x-ray patterns using the FULLPROF package program [31] indicated that all crystals were single phase without detectable impurities. The oxygen content of all samples was determined by cerimetric titration with cerium (IV) sulfate and Mohr´s salt [32]. This analysis was repeated three times for each sample and the standard deviation in δ is estimated to be ± 0.02. The studied single crystals display an oxygen stoichiometry and nominal average Co oxidation state of $La_{1.6}Ca_{0.4}CoO_{4.04}$ ($Co^{2.48+}$), $La_{1.5}Ca_{0.5}CoO_{4.02}$ ($Co^{2.54+}$), $La_{1.4}Ca_{0.6}CoO_{3.94}$ ($Co^{2.48+}$), $La_{1.3}Ca_{0.7}CoO_{3.9}$ ($Co^{2.5+}$), and $La_{1.5}Sr_{0.5}CoO_{3.99}$ ($Co^{2.48+}$). On the other hand, the reference samples have larger nonstoichiometric compositions, $La_2CoO_{4.2}$ ($Co^{2.4+}$) and $LaSrCoO_{3.91}$ ($Co^{2.82+}$).

Synchrotron x-ray-diffraction patterns were measured at the BL04-MSPD beam line [33] at the ALBA synchrotron radiation facility. The samples were loaded in a borosilicate glass capillary (diameter of 0.5 mm) and kept spinning during data acquisition. A short wavelength, $\lambda = 0.3259$ Å, was selected to reduce absorption. The value of λ was calibrated using standard silicon. The patterns were collected at room temperature. The standard acquisition time to refine unit cells was about 30 min, but a total acquisition time of 2 h/pattern was used to perform a full structural characterization. All the studied samples are indexed in the tetragonal $I4/mmm$ lattice at room temperature. Lattice parameters for the three $x = 0.4$, 0.5, and 0.6 samples are very similar within 1% variations and exhibit the expected contraction with increasing the Ca content. The only exception is $La_2CoO_{4.2}$, which results in the orthorhombic $Bmab$ crystal structure due to the incorporation of the extra oxygen atoms in the interstitial positions of the LaO layer of this layered perovskite.

Room-temperature RXS experiments at the Co K edge (7.709 keV) were carried out at the BM02-D2AM beam line [34] at the European Synchrotron Radiation Facility (ESRF). The incident beam was monochromatized by a Si(1,1,1) double crystal, energy resolution being 1 eV at the Co K edge. The beam was linearly polarized (99%) with the polarization vector perpendicular to the scattering plane. Single crystals were cut and polished with the surface perpendicular to the $[1, 1, 0]_t$ direction with the exception of $La_{1.3}Ca_{0.7}CoO_{3.9}$, which was cut along the $[0, 0, 1]_t$ direction. The $(h/2, h/2, l)_t$ and $(h/4, h/4, 0)_t$ superstructure reflections were checked. The energy dependence of the scattered intensity across the Co K edge was measured. Azimuthal-dependent scans at the resonance energy were measured by rotating the sample around

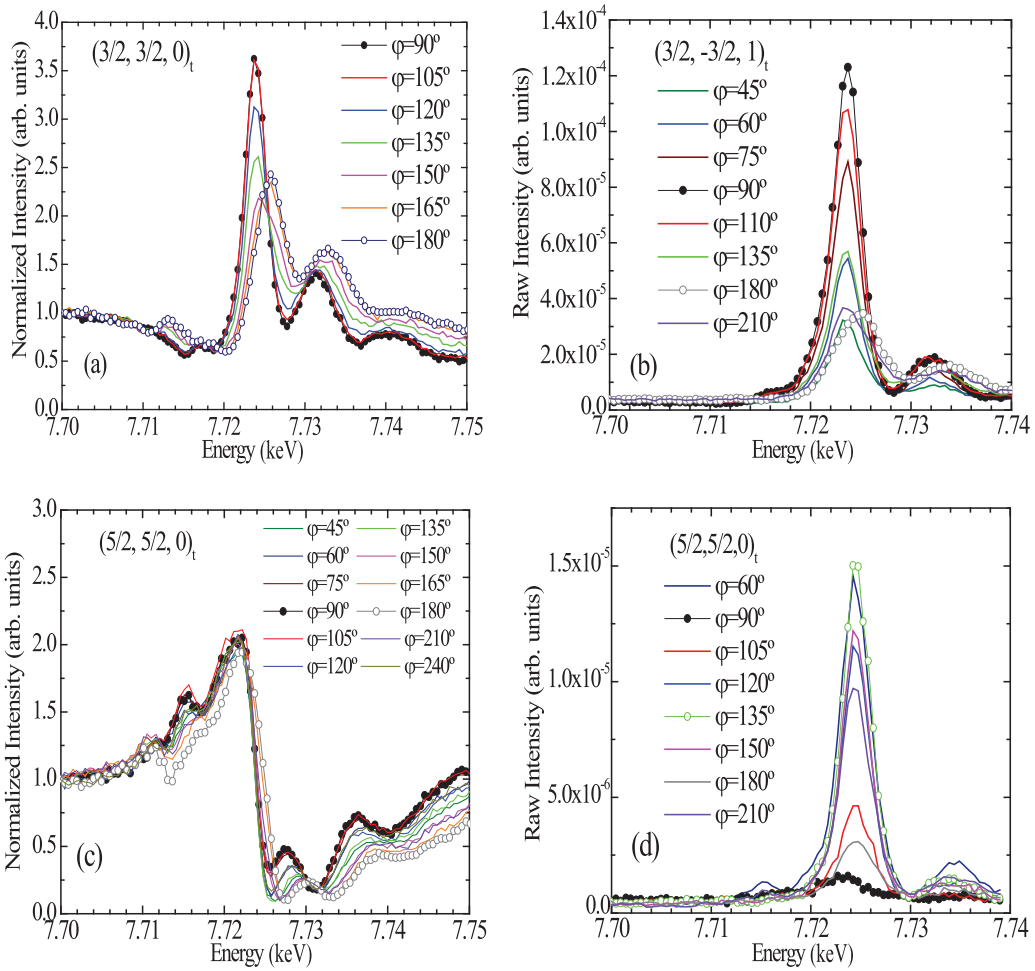

FIG. 1. Energy dependence of resonant reflections near the Co K edge as a function of the azimuthal angle without absorption correction: (a) $(3/2,\ 3/2,\ 0)_t$, (b) $(3/2,\ -3/2,\ 1)_t$, and (c) $(5/2,\ 5/2,\ 0)_t$ in the σ-σ' polarization channel and (d) $(5/2,\ 5/2,\ 0)_t$ in the σ-π' polarization channel for the $La_{1.5}Ca_{0.5}CoO_{4.02}$ single crystal.

the scattering vector Q in a range of $\sim 180°$. The crystals, with the exception of $La_{1.3}Ca_{0.7}CoO_{3.9}$, were mounted in such a way that for an azimuthal angle $\varphi = 90°$ the electric field of the σ-polarized x-ray beam is parallel to the c axis ($\mathbf{E} \parallel \mathbf{c}$). Accordingly, $\mathbf{E} \perp \mathbf{c}$ for $\varphi = 0$ or 180°. The polarization of the scattered x-ray beam was analyzed using a Cu(2,2,0) crystal, which allows the measurement of the σ-σ' and σ-π' channels independently. An empirical analysis of the RXS data, once they have been corrected for self-absorption, was carried out by the experimental determination of the resonant atomic scattering factor tensor. Theoretical simulations of the resonant reflections were carried out by the FDMNES code [35] in order to estimate the magnitude of the local structural distortions associated with the CO.

Polarized x-ray absorption near-edge structure (XANES) spectra for the $La_{2-x}Ca_xCoO_{4\pm\delta}$ ($x = 0$ and 0.5) single crystals and a $LaSrCoO_{3.91}$ oriented pellet were recorded at the BM23 beam line [36] at the ESRF. Measurements were collected at room temperature in fluorescence mode by means of a Camberra 13-elements Ge solid-state detector in two configurations. The in-plane configuration corresponds to the crystal surface (ab plane in this case) almost perpendicular to the incident beam (80°) and the out-of-plane configuration corresponds to the crystal surface almost parallel to the incident beam, i.e., the angle between the electric-field vector $\mathbf{E}$ and the c axis is 15°. The complete polarization-dependent x-ray absorption and x-ray emission spectroscopic study at the Co K edge of the $La_{2-x}Ca(Sr)_xCoO_{4\pm\delta}$ series will be published elsewhere.

III. RESULTS AND DISCUSSION

A. Experimental results

We have explored the occurrence of superstructure reflections by means of reciprocal-lattice scans along the $[h,\ h,\ l]_t$ directions. Only $(h/2,\ h/2,\ l)_t$ reflections were detected while $(h/4,\ h/4,\ l)_t$ ones were not observed at room temperature in agreement with previous results [29]. First, our paper focuses on the $La_{1.5}Ca_{0.5}CoO_{4.02}$ sample. Figures 1(a) and 1(b) show the energy dependence of the scattered intensity across the Co K edge in the σ-σ' channel and at different azimuthal angles (φ) for the $(3/2,\ 3/2,\ 0)_t$ and $(3/2,\ -3/2,\ 1)_t$ reflections, respectively. We observe scattered intensity at energies below the Co K edge, which comes from the atomic displacements out of the $I4/mmm$ symmetry (Thomson scattering). Therefore, these reflections are allowed by the crystal symmetry of

the room-temperature phase. The scattered intensity of both reflections enhances at photon energies close to the Co K edge, i.e., they exhibit a broad main peak, which comes from the difference between the resonant atomic scattering factors of Co atoms located in nonequivalent crystallographic sites. The similar behavior in both reflections indicates that this feature does not depend on the value of the l index (odd or even). The resonant intensity, however, depends on the azimuthal angle reaching the maximum value at $\varphi = 90^\circ$ and the minimum at about 180°. On the other hand, Fig. 1(c) displays the results obtained for the $(5/2, 5/2, 0)_t$ reflection. In this case, the scattered intensity in the σ-σ' channel shows a strong decrease at the Co K edge. Similar results were obtained (not shown here) for $(5/2, -5/2, 1)_t$ and $(5/2, 5/2, 2)_t$ reflections. The change in sign of the RXS spectra for different h indices in $(h/2, h/2, l)_t$ reflections has also been observed in the RXS studies of layered cobaltites [28], manganites [13], and iron ferrites [37]. The different behavior in the energy-dependent spectra for the $(3/2, 3/2, l)_t$ and the $(5/2, 5/2, l)_t$ reflections indicates that the resonant part of the atomic scattering factor of Co atoms is in phase for $h = 3/2$ and out of phase for $h = 5/2$ with the Thomson scattering term. Additionally, the spectra line shape slightly changes with the azimuthal angle for all the reflections. This moderate dependence arises from the tetragonal anisotropy at the Co sites in the crystal structure.

Figure 1(d) shows the energy-dependent spectra of the $(5/2, 5/2, 0)_t$ reflection in the σ-π' channel at different azimuthal angles. This reflection shows a main resonance at the Co K edge with a strong azimuthal dependence with a $\pi/2$ periodicity. As expected, no Thomson scattering is observed in this channel. The observation of a resonant signal in this polarization channel is also a signature of the local anisotropy of the resonant atomic scattering factors of the individual Co atoms as we will further explain in the next section.

As mentioned above, we have also explored the occurrence of $(h/4, h/4, l)_t$ reflections with the aim of comparing to the isostructural $La_{0.5}Sr_{1.5}MnO_4$ compound [13]. No scattered intensity was observed at any energy either in the σ-σ' or in the σ-π' polarization channels at room temperature. The absence of a σ-σ' signal demonstrates that these reflections are forbidden by symmetry and the lack of a σ-π' signal indicates the absence of a local anisotropy ordering [38–40] for these reflections in contrast to the behavior observed in related layered manganites [13].

Similar results have been obtained for the rest of the $La_{2-x}Ca_xCoO_{4\pm\delta}$ samples ($x = 0.4$, 0.6 and 0.7). Figures 2(a) and 2(b) compare the spectra of representative $(h/2, h/2, 0)_t$ reflections for $x = 0.4$, 0.5, and, 0.6 samples for two values of the azimuthal angle, $\varphi = 90$ and 0°. Qualitatively, the three samples show similar energy and azimuthal dependencies. In Fig. 2(a), we note an energy shift of the main resonance peak depending on the azimuthal angle. In this way, the peak occurs at ~7.725 keV for $\varphi = 90^\circ$ ($\mathbf{E} \parallel \mathbf{c}$) and about 2 eV above for $\varphi = 0^\circ$ ($\mathbf{E} \perp \mathbf{c}$). A similar energy shift is observed in the first minimum of the spectra of Fig. 2(b). On the other hand, some differences are noticeable in the intensity of the main resonance. As can be seen in Fig. 2(a), the $I_{\mathbf{E}\parallel\mathbf{c}}/I_{\mathbf{E}\perp\mathbf{c}}$ ratio for the $(3/2, 3/2, 0)_t$ reflection is 2, 1.5, and 1.8 for $x = 0.4$, 0.5, and 0.6 samples, respectively. The lowest difference in

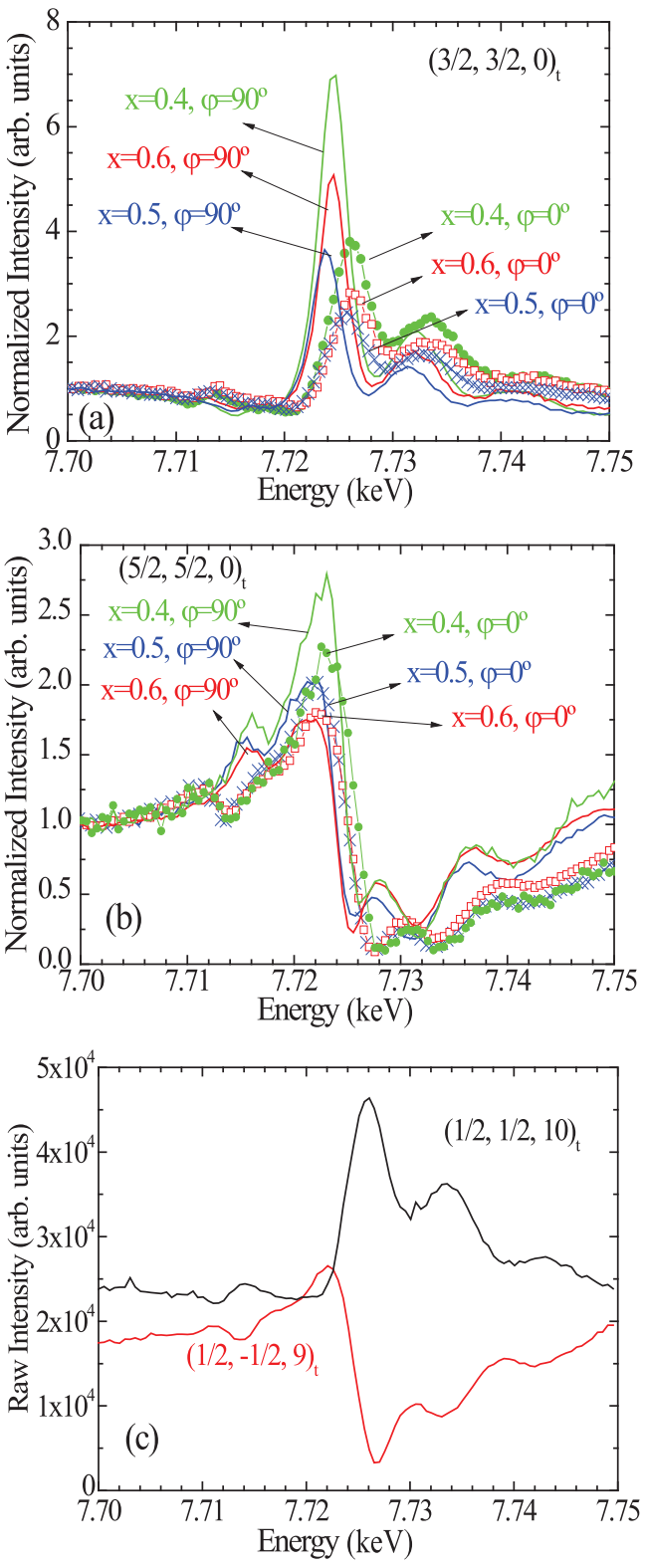

FIG. 2. Energy dependence of the resonant $(3/2, 3/2, 0)_t$ (a) and $(5/2, 5/2, 0)_t$ (b) reflections for $La_{2-x}Ca_xCoO_{4\pm\delta}$ ($x = 0.4, 0.5, 0.6$) samples at two azimuthal angles with $\mathbf{E} \parallel \mathbf{c}$ ($\varphi = 90^\circ$) and $\mathbf{E} \perp \mathbf{c}$ ($\varphi = 0^\circ$) in the σ-σ' channel without absorption correction. (c) Energy dependence of the resonant $(1/2, -1/2, 9)_t$ and $(1/2, 1/2, 10)_t$ reflections for the $La_{1.3}Ca_{0.7}CoO_{3.9}$ sample at $\varphi = 90^\circ$ in the σ-σ' channel without absorption correction.

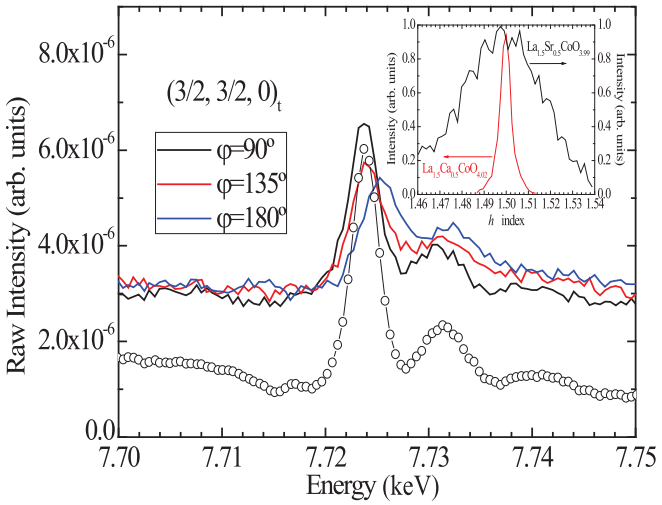

FIG. 3. Energy dependence of the raw intensity at the $(3/2, 3/2, 0)_t$ reflection in the σ-σ' channel without absorption correction for $La_{1.5}Sr_{0.5}CoO_{3.99}$ (solid lines). The energy dependence of the raw intensity at the same reflection and $\varphi = 90°$ in the σ-σ' channel without absorption correction for $La_{1.5}Ca_{0.5}CoO_{4.02}$ divided by a factor 50 is also shown for comparison (open circles). Inset:h scans through the $(h, h, 0)_t$ CO reflections for the $La_{1.5}Ca_{0.5}CoO_{4.02}$ and $La_{1.5}Sr_{0.5}CoO_{3.99}$ samples normalized at the peak position. Correlation lengths were extracted from the scans by a Lorentzian fit to be $\xi(La_{1.5}Ca_{0.5}CoO_{4.02}) \sim 219$ Å and $\xi(La_{1.5}Sr_{0.5}CoO_{3.99}) \sim 21$ Å.

the peak intensity as a function of the azimuthal angle is then shown by the nominal half-integer valence ($x = 0.5$) sample. Moreover, Fig. 2(c) displays the energy-dependent spectra of the $(1/2, -1/2, 9)_t$ and $(1/2, 1/2, 10)_t$ reflections for the $La_{1.3}Ca_{0.7}CoO_{3.9}$ crystal. In this case, the electric-field polarization vector **E** is nearly parallel to the ab plane and a different sign in the interference between the Thomson scattering and the resonant scattering of Co atoms occurs for l odd (destructive) or even (constructive) in the σ-σ' channel. We note that these reflections of the $x = 0.7$ sample do not show azimuthal dependence, as expected from the fact that **E** lies close to the ab plane (within 8°) and the lack of anisotropy in the ab plane.

It is noteworthy that we do not find resonant superlattice $(h \pm \varepsilon, h \pm \varepsilon, 0)_t$ reflections with a modulation $2\varepsilon = 1 - x$ in the $La_{2-x}Ca_xCoO_{4\pm\delta}$ samples ($x = 0.4$, 0.6, and 0.7) opposite to the results found in layered manganites, where the observed resonant reflections exhibited a modulation vector following the doping rate [26,27]. Instead, here layered cobaltites show a strong stabilization of the $(h/2, h/2, 0)_t$ reflection well out of the nominal doping $x = 0.5$, in agreement with previous reports [25]. This result reflects different structural effects of the hole doping for both layered structures as we will discuss later on.

We have performed the same study on the $La_{1.5}Sr_{0.5}CoO_{4.02}$ sample. Figure 3 shows the energy dependence of the raw scattered intensity in the σ-σ' channel at the $(3/2, 3/2, 0)_t$ reflection in $La_{1.5}Sr_{0.5}CoO_{3.99}$ for selected azimuthal angles. The resulting spectra behave in a similar way to those of the Ca-based samples across the Co K edge so a similar CO pattern takes place. The only remarkable difference is the magnitude of the resonant intensities, which is about 50 times smaller in the Sr-doped sample than in the Ca-doped one (see Fig. 3) taking into account that the intensity of the fundamental (2,2,0) reflections is similar for both samples. Moreover, the resonant reflections are also much broader in the Sr-doped sample, as shown in the inset of Fig. 3, indicating a much shorter correlation length of the CO for the Sr half-doped sample. For this reason, the analysis of experimental data will be focused on Ca-based compounds. Regarding the azimuthal dependence of the scattered intensity, Fig. 4 compares the evolution of the intensity at a fixed energy of 7.7245 keV for the $(3/2, 3/2, 0)_t$ reflection in the σ-σ' channel and the $(5/2, 5/2, 0)_t$ reflection in the σ-π' channel for the $La_{2-x}Ca_xCoO_{4\pm\delta}$ samples with $x =$ 0.4, 0.5, and 0.6. As we can observe, the same azimuthal dependence is exhibited by the three samples with a π periodicity for the σ-σ' scattered intensity, being the maximum intensity observed at $\varphi = 90°$ (**E** ∥ **c**). For the σ-π' scattered intensity, the three samples show a $\pi/2$ periodicity with the maximum intensity at $\varphi = 45°$. Therefore, a single theoretical model

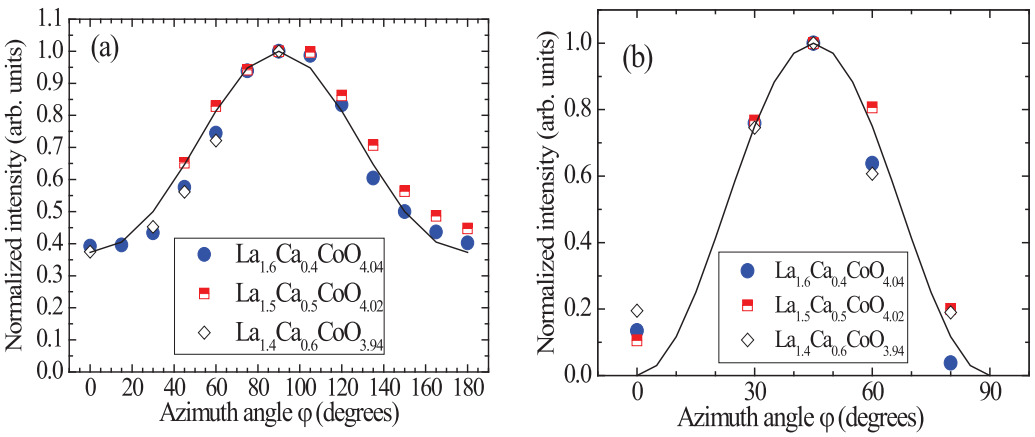

FIG. 4. Normalized azimuthal dependence of the resonant intensity at $E = 7.7245$ keV for (a) the $(3/2, 3/2, 0)_t$ reflection in the σ-σ' channel and (b) the $(5/2, 5/2, 0)_t$ reflection in the σ-π' channel for $La_{2-x}Ca_xCoO_{4\pm\delta}$ ($x = 0.4$, 0.5 and 0.6). The data were normalized to the values at $\varphi = 90$ and at 45° for the σ-σ' and σ-π' resonant intensities, respectively. The solid lines are the results of calculations using Eqs. (1) and (2), as discussed in the text.

should be able to describe the RXS properties of the three samples.

B. Theoretical model and analysis

The resonant reflections observed in $La_{1.5}Ca_{0.5}CoO_{4.02}$ are typical of a checkerboard ordering of two local geometrical and electronically different Co atoms. This implies that this compound is no longer tetragonal. As indicated in the introduction, the symmetry of the distorted structure is $A2mm$, and the transformation matrix relating the tetragonal cell to the orthorhombic one is

$$\begin{pmatrix} a_o \\ b_o \\ c_o \end{pmatrix} = \begin{pmatrix} 1 & 1 & 0 \\ 1 & -1 & 0 \\ 0 & 0 & 1 \end{pmatrix} \begin{pmatrix} a_t \\ b_t \\ c_t \end{pmatrix}.$$

According to this matrix, the tetragonal $(h/2,\ h/2,\ l)_t$ and $(h/2,\ -h/2,\ l)_t$ reflections transform into the orthorhombic $(h,\ 0,\ l)_o$ and $(0,\ k,\ l)_o$ ones, respectively. Due to the symmetry conditions of the $A2mm$ space group, the $(0,\ k,\ l)_o$ reflections are only allowed for $k + l =$ even while the $(h,\ 0,\ l)_o$ ones are allowed for $l =$ even. Therefore, no mixture between these two types of reflections due to the twinning is expected for either h or k odd that is the case for all the reflections measured in this paper. The structure factor for these allowed $(h,\ 0,\ 0)_o$ $(h =$ odd) and $(0,\ k,\ 1)_o$ $(k =$ odd) reflections is given by $F = F_0 + 2(f_{Co1} - f_{Co2})$, where F_0 stands for the Thomson structure factor coming from atomic shifts away from the tetragonal position of the undistorted tetragonal cell, and f_{Coi} $(i = 1,2)$ is the resonant atomic scattering factor for each of the two nonequivalent Co atoms in the orthorhombic cell. We use the dipole approximation to describe the resonant atomic scattering factor tensor [38–40]. This approach is fully justified because the main resonances are observed at the Co K edge and spectroscopic features arising from higher-order transitions (as quadrupole) are generally observed at the pre-edge energy. Within this approach, the resonant atomic scattering factor can be expressed as $\boldsymbol{F_{\varepsilon\varepsilon'}} = \overrightarrow{\epsilon'} \cdot \hat{\boldsymbol{F}} \cdot \vec{\epsilon}$. Here, $\overrightarrow{\varepsilon'}$ and $\vec{\varepsilon}$ are the scattered and incident electric polarization vectors, respectively, and $\hat{F}$ is a second rank symmetric tensor, the specific form of which only depends on the site symmetry of the resonant atoms in the crystal. Taking into account the very small orthorhombic distortion of the cell (not detectable by conventional x-ray diffraction) we can approach a tetragonal symmetry for the two Co atoms. Thus, the resonant atomic scattering factor tensor for each of them is diagonal. Assuming the lattice vector (**a**, **b,** and **c**) directions as the tensor axes, $f_{xx} = f_{yy}$ and the resonant atomic scattering factor tensor can be written as

$$f_{\mathrm{Co1}} = \begin{pmatrix} f^1_{xx} & 0 & 0 \\ 0 & f^1_{xx} & 0 \\ 0 & 0 & f^1_{zz} \end{pmatrix} \text{ and } f_{\mathrm{Co2}} = \begin{pmatrix} f^2_{xx} & 0 & 0 \\ 0 & f^2_{xx} & 0 \\ 0 & 0 & f^2_{zz} \end{pmatrix}.$$

Thus, the resonant part of the structure factor is given by

$$F(h,k,l)_{\epsilon\epsilon'} = \epsilon' \begin{pmatrix} \Delta f_{\mathrm{xx}} & 0 & 0 \\ 0 & \Delta f_{\mathrm{xx}} & 0 \\ 0 & 0 & \Delta f_{\mathrm{zz}} \end{pmatrix} \epsilon$$

$$\text{with } \Delta f_{xx} = f^1_{xx} - f^2_{xx} \text{ and } \Delta f_{zz} = f^1_{zz} - f^2_{zz}.$$

For the $(h,\ 0,\ 0)_o$ $(h =$ odd) reflections in the σ-σ' and σ-π' channels the general structure factors are

$$F(h,0,\ 0)_{\sigma\sigma'} = F_0(h,0,\ 0) + 2[\Delta f_{xx}\cos^2\varphi + \Delta f_{zz}\sin^2\varphi] \quad (1)$$

and

$$\begin{aligned} F(h,0,\ 0)_{\sigma\pi'} &= \sin 2\varphi \sin\theta[\Delta f_{xx} - \Delta f_{zz}] \\ &= \sin 2\varphi \sin\theta\left[\left(f^1_{xx} - f^1_{zz}\right) - \left(f^2_{xx} - f^2_{zz}\right)\right]. \end{aligned} \quad (2)$$

As usual, φ stands for the azimuthal angle, θ is the Bragg angle, and F_0 $(h,\ 0,\ 0)$ is the Thomson scattering factor, which can be either positive or negative in sign depending on the value of the h index.

The calculation of the structure factor for the $(0,\ k,\ l)_o$ $(k =$ odd) reflections is, however, not so direct since the incident and scattered polarization vectors cannot be described as the in-plane and out-of-plane components (these are not specular reflections). For instance, we have calculated the structure factor for the $(0,\ k,\ 1)_o$ $(k =$ odd) reflection in the

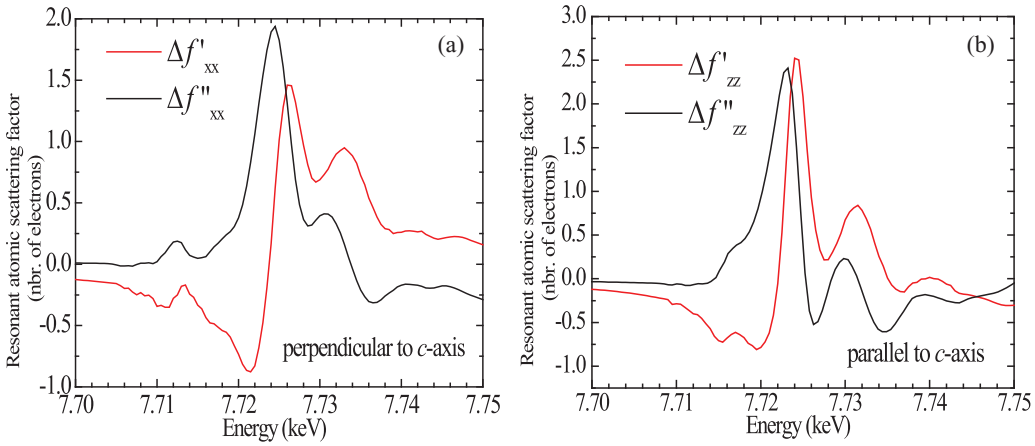

FIG. 5. (a) The real $(\Delta f'_{xx})$ and imaginary $(\Delta f''_{xx})$ terms of the difference of the resonant atomic scattering factors for Co1 and Co2 atoms when the polarized electric field **E** is perpendicular to the c axis. (b) The real $(\Delta f'_{zz})$ and imaginary $(\Delta f''_{zz})$ components of the difference of the resonant atomic scattering factors for Co1 and Co2 atoms when the polarized electric field **E** is parallel to the c axis.

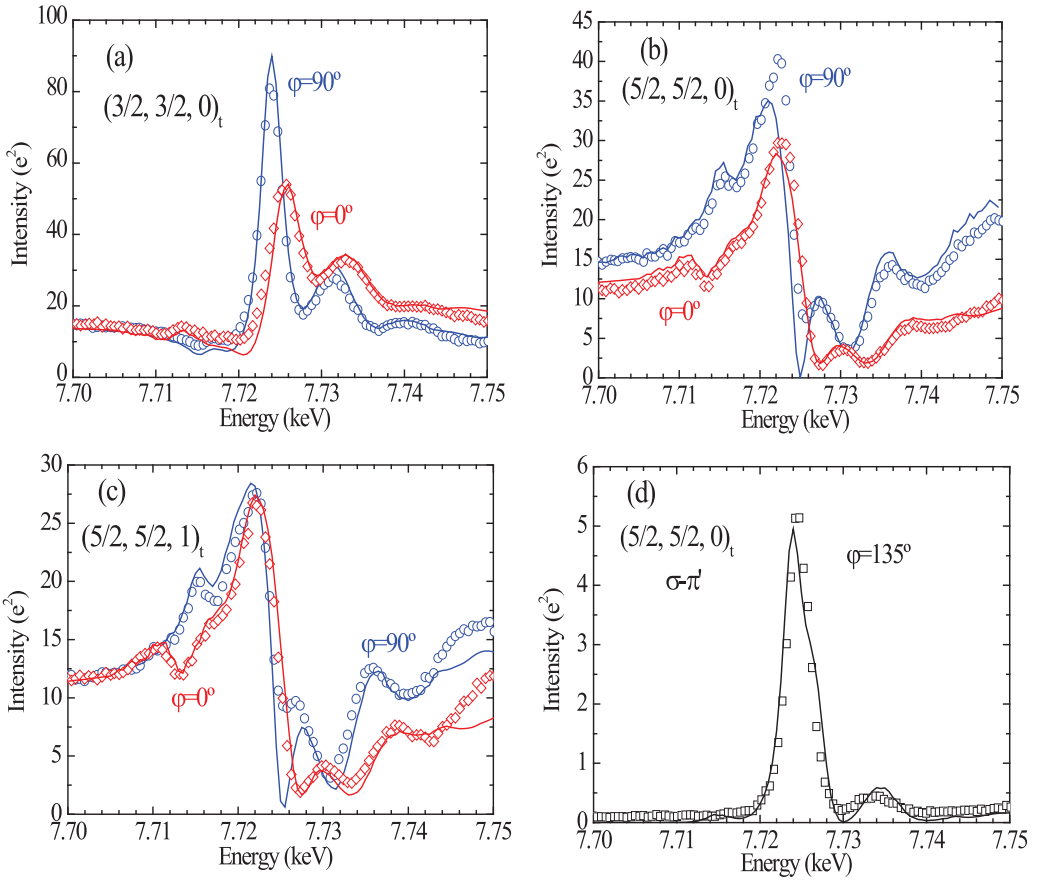

FIG. 6. Comparison between the self-absorption corrected energy dependence of resonant reflections (points) and the simulated spectra (lines) obtained from the empirical analysis outlined in the text for the $La_{1.5}Ca_{0.5}CoO_{4.02}$ sample. (a) Data for $(3/2, 3/2, 0)_t$ reflection in the σ-σ' channel at $\varphi = 90°$ ($\mathbf{E} \parallel \mathbf{c}$) and $\varphi = 0°$($\mathbf{E} \perp \mathbf{c}$). (b) Data for $(5/2, 5/2, 0)_t$ and (c) for $(5/2, 5/2, 1)_t$ reflections in the same polarization channel and azimuthal angles. (d) Data for $(5/2, 5/2, 0)_t$ reflection in the σ-π' channel at $\varphi = 135°$.

σ-σ' channel:

$$F(0, k, 1)_{\sigma\sigma'} = F_0(0,k,1) + 2[\Delta f_{xx}\cos^2\varphi + \Delta f_{xx}\sin^2\psi\sin^2\varphi + \Delta f_{zz}\cos^2\psi\sin^2\varphi]. \quad (3)$$

Here Ψ is the angle between $[0, k, 1]_o$ and $[0, 1, 0]_o$ directions. The Ψ values for the $(0, 3, 1)_o$ and $(0, 5, 1)_o$ reflections are 8.347 and 5.03°, respectively, so we can assume $\sin^2\Psi \sim 0$ and $\cos^2\Psi \sim 1$ as a first approximation. Within this approach, we obtain the same expression for the structure factor of $(h, 0, 0)_o$ and $(0, k, 1)_o$ reflections. Again the sign of the Thomson scattering term F_0 $(0, k, 1)$ can be either positive of negative depending on the value of the k index.

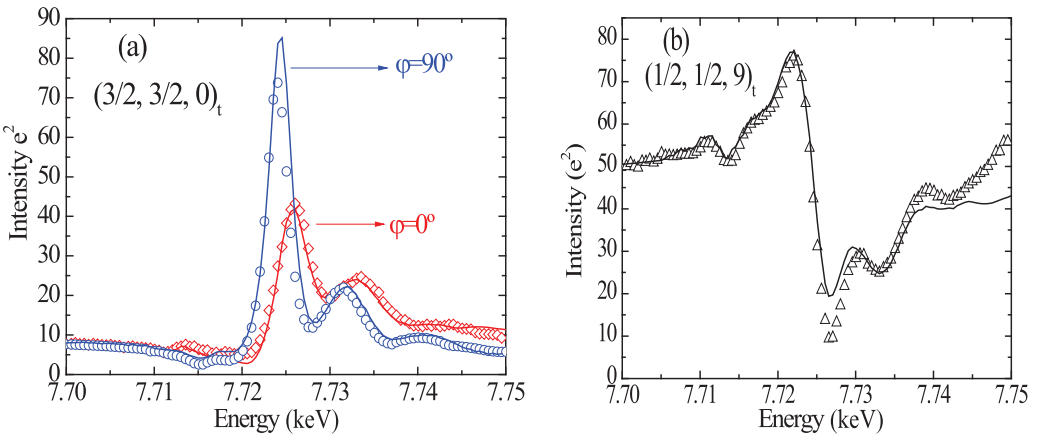

FIG. 7. Comparison between the self-absorption corrected energy dependence of resonant reflections (points) and the simulated spectra (lines) obtained from the empirical analysis outlined in the text in the σ-σ' channel for (a) the $(3/2, 3/2, 0)_t$ reflection of the $La_{1.6}Ca_{0.4}CoO_{4.04}$ sample at $\varphi = 90°$ ($\mathbf{E} \parallel \mathbf{c}$) and $\varphi = 0°$ ($\mathbf{E} \perp \mathbf{c}$) and (b) the $(1/2, 1/2, 9)_t$ of the $La_{1.3}Ca_{0.7}CoO_{3.9}$ sample at $\varphi = 90°$.

A different problem is the calculation of the structure factors for the $(0, 1, 9)_o$ and the $(1, 0, 10)_o$ reflections used in the $La_{1.3}Ca_{0.7}CoO_{3.9}$ sample. In this crystal, the surface normal corresponds to the [001] direction so the incident polarized **E** field lies close to the *ab* plane and therefore

$$F(0,1,9)_{\sigma\sigma'} = F_0(0,1,9) + 2\Delta f_{xx},$$
$$F(1,0,10)_{\sigma\sigma'} = F_0(1,0,10) + 2\Delta f_{xx}.$$

Here, the sign change in the Thomson scattering term depends on the *l* index being odd or even.

According to the previous expressions, the Thomson scattering term is positive for the $(3, 0, 0)_o$, $(0, 3, 1)_o$, and $(1, 0, 10)_o$ reflections, that is in phase with the resonant scattering term of Co atoms and a positive resonance or peak is expected in the energy dependence at the Co K edge, as experimentally observed (see Figs. 1 and 2). On the other hand, the Thomson scattering term is negative for the $(5, 0, 0)_o$ and $(0, 1, 9)_o$ reflections and the two terms, nonresonant and resonant, are out of phase so an intensity decrease or valley is observed at the edge energy. The azimuthal dependence of the σ-σ' and σ-π' resonant intensities is well reproduced by the sinusoidal functions given in Eqs. (1) and (2), respectively (Fig. 4), and shows the anisotropy of the Co resonant atomic scattering factor between the *c*-axis and the *ab*-plane components.

The two components of the resonant atomic scattering factor, Δf_{xx} and Δf_{zz} [Eq. (1)], can be retrieved from the self-absorption corrected experimental intensity of the $(3, 0, 0)_o$ and $(5, 0, 0)_o$ reflections in the σ-σ' channel for $\varphi = 0$ and 90°, respectively. Taking into account that for these two reflections $F_0(3, 0, 0) = F_0 \sim -F_0(5, 0, 0)$, for $\varphi = 0°$,

$$\begin{aligned} I(3, 0, 0)_o &= [F_0 + 2\Delta f_{xx}]^2 \\ &= [(F_0 + 2\Delta f'_{xx}) + i2\Delta f''_{xx}]^2 \\ &= F_0^2 + 4\Delta f'^2_{xx} + 4F_0\Delta f'_{xx} + 4\Delta f''^2_{xx} \end{aligned}$$

and

$$\begin{aligned} I(5, 0, 0)_o &= [-F_0 + 2\Delta f_{xx}]^2 \\ &= [(-F_0 + 2\Delta f'_{xx}) + i2\Delta f''_{xx}]^2 \\ &= F_0^2 + 4\Delta f'^2_{xx} - 4F_0\Delta f'^2_{xx} + 4\Delta f''^2_{xx}. \end{aligned}$$

Therefore, $I(3, 0, 0)_o + I(5, 0, 0)_o = 2F_0^2 + 8(\Delta f'^2_{xx} + \Delta f''^2_{xx})$ and $I(3, 0, 0)_o - I(5, 0, 0)_o = 8F_0\Delta f'_{xx}$.

Similar expressions are deduced for $\varphi = 90°$ but changing Δf_{xx} by Δf_{zz}. Therefore, the difference of the two intensities is proportional to the difference of the real parts of the two resonant atomic scattering factors for Co1 and Co2. The proportional factor $8F_0$ was determined by the relationship between the nonresonant intensity of the $(3, 0, 0)_o$ and $(5, 0, 0)_o$ reflections and the allowed $(2, 0, 0)_o$ Bragg reflection. The difference of the imaginary parts of the two resonant atomic scattering factors for Co1 and Co2 is then determined by an iterative Kramers-Kronig transformation of the experimentally obtained differential signals $\Delta f'_{xx}$ (or $\Delta f'_{zz}$). Figure 5 shows the real and imaginary components of the difference of the two resonant atomic scattering factors parallel and perpendicular to the *c* axis.

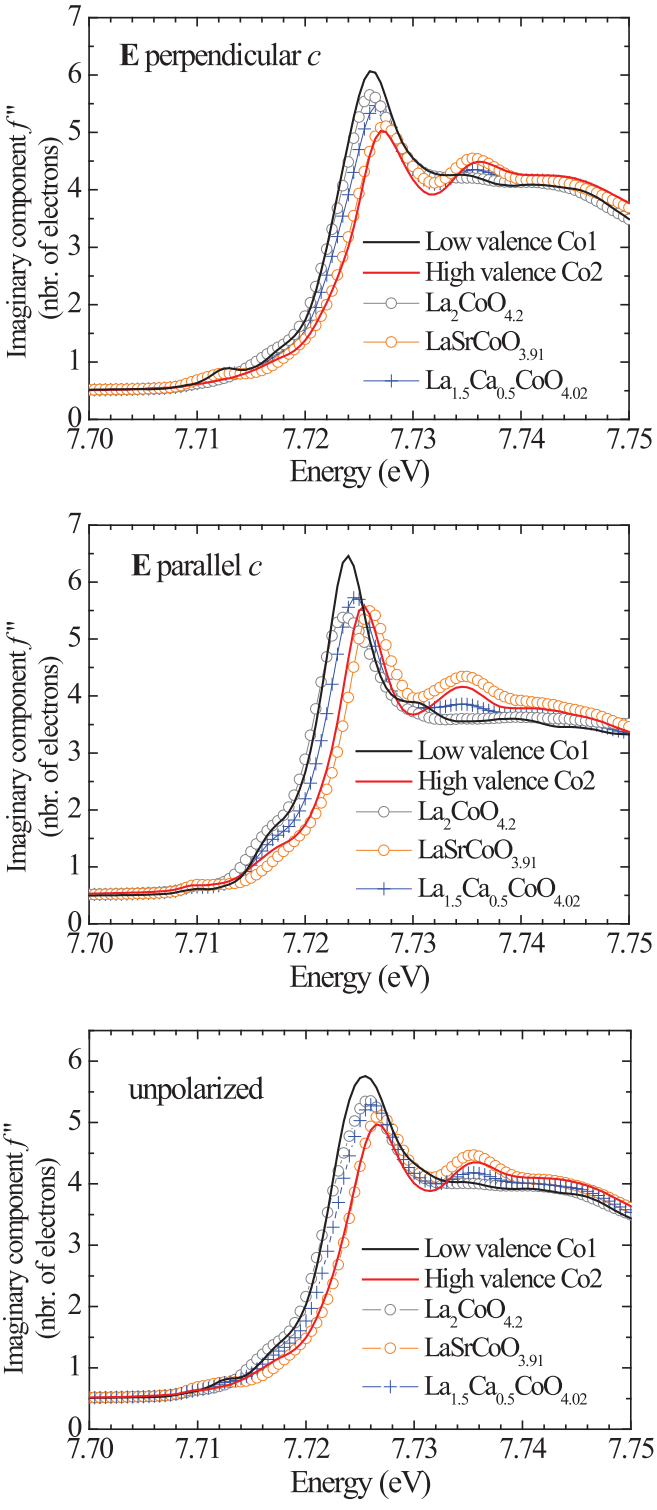

FIG. 8. Imaginary $f''(E)$ components of the resonant atomic scattering factor of the two Co sites with the electric field parallel to the *ab* plane (upper panel), the electric field parallel to the *c* axis (middle panel), and unpolarized (bottom panel) compared to the corresponding experimental XANES spectra of the $La_2CoO_{4.2}$, $La_{1.5}Ca_{0.5}CoO_{4.02}$, and $LaSrCoO_{3.91}$ samples normalized to electron units.

Making use of these experimental $\Delta f'_{xx}$ (or $\Delta f'_{zz}$) and $\Delta f''_{xx}$ (or $\Delta f''_{zz}$) terms and the estimated Thomson scattering intensity, we have simulated the energy dependence of the structure

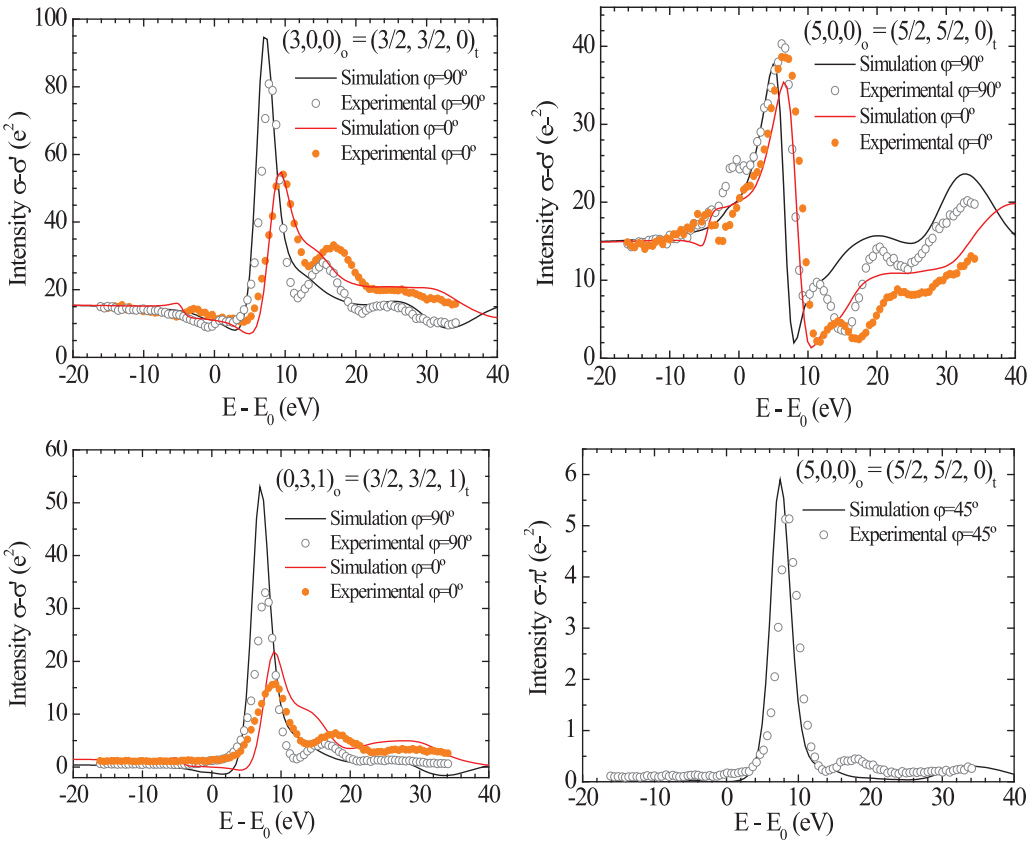

FIG. 9. Energy dependence of theoretical simulated intensities (full line) and self-absorption corrected experimental RXS spectra (dots) for the resonant reflections in $La_{1.5}Ca_{0.5}CoO_{4.02}$ around the Co K edge. Theoretical simulations are performed with the oxygen atom displacements relative to the $A2mm$ structure of Cd_2CoO_4 given in the text.

factor for the resonant reflections in all the $La_{2-x}Ca_xCoO_{4\pm\delta}$ ($x = 0.4$, 0.5, 0.6, and 0.7) samples. Figures 6 and 7 show the comparison between the energy dependence of the simulated intensity and the corresponding experiment for several resonant reflections in $La_{1.5}Ca_{0.5}CoO_{4.02}$ and $La_{2-x}Ca_xCoO_{4\pm\delta}$ ($x \neq 0.5$) samples, respectively. Hereafter, all experimental spectra have been corrected for self-absorption on the basis of the Lambert-Beer law. For that, we have multiplied the raw RXS spectra by μd with μ the linear absorption coefficient. The value of d has been determined so as to yield the average intensity roughly equal well below and above the absorption edge [37]. As it is shown, the agreement is quite good for all of the resonant reflections.

The fact that Δf_{xx} and Δf_{zz} are greater than zero implies that the atomic scattering factor for the Co1 site is greater than the one for the Co2 site at energies close to the absorption edge, i.e., the x-ray-absorption spectra for the Co1 atom are shifted to lower energies than those for the Co2 one in both the x and z directions. This agrees with an expansion of the $Co1O_6$ coupled to a compression of the $Co2O_6$ octahedra. We also observe σ-π' intensity for $(h,0,0)_o$ and $(0,k,l)_o$ (h, k = odd) reflections. As it can be deduced from Eq. (2), the occurrence of these reflections in the σ-π' channel is due to the fact that $(f^1_{xx} - f^1_{zz})$ and/or $(f^2_{xx} - f^2_{zz})$ are different from zero, which confirms the presence of tetragonal anisotropy for at least one of the two Co sites. Taking in mind that we have experimentally obtained the difference between the imaginary parts of the resonant atomic scattering factors of the two Co sites and the XANES spectrum of $La_{1.5}Ca_{0.5}CoO_{4.02}$ corresponds to the sum, we can deduce the individual polarized XANES spectra of each of the two nonequivalent Co atoms. In this way, $f''_{Co1} = f''[\text{XANES}(x = 0.5) + 0.5\,\Delta f'']$ and $f''_{Co2} = f''[\text{XANES}(x = 0.5) - 0.5\,\Delta f'']$. Figure 8 shows the obtained polarized XANES spectra for the two Co sites compared to those of the $La_{1.5}Ca_{0.5}CoO_{4.02}$, $La_2CoO_{4.2}$, and $LaSrCoO_{3.91}$ samples. The polarized XANES spectra of Co1 and Co2 sites with the electric field parallel to the ab plane (upper panel in Fig. 8) are quite similar to the polarized XANES spectra of $La_2CoO_{4.2}$ and $LaSrCoO_{3.99}$, respectively. However, differences in either the energy position of the absorption edge or the energy line shape are observed for the polarized XANES spectra with the electric field parallel to the c axis (middle panel in Fig. 8) above all for the Co1 site compared to the reference $La_2CoO_{4.2}$ sample. The incorporation of extra oxygen atoms in $La_2CoO_{4+\delta}$ mainly occurs in interstitial positions along the c axis [41]. This corresponds to the apical oxygens and explains the fact that the main differences are found for the polarized XANES spectra along the c axis. We have then used the unpolarized XANES spectra shown in the bottom panel of Fig. 8 to determine the chemical shift between the Co1 and Co2 sites, which results to be about 1.6 eV. Here, the energy position of the absorption edge (E_0) is taken at the maximum of the derivative of the normalized f'' signal. Taking into account that the chemical shift between Co^{2+} and

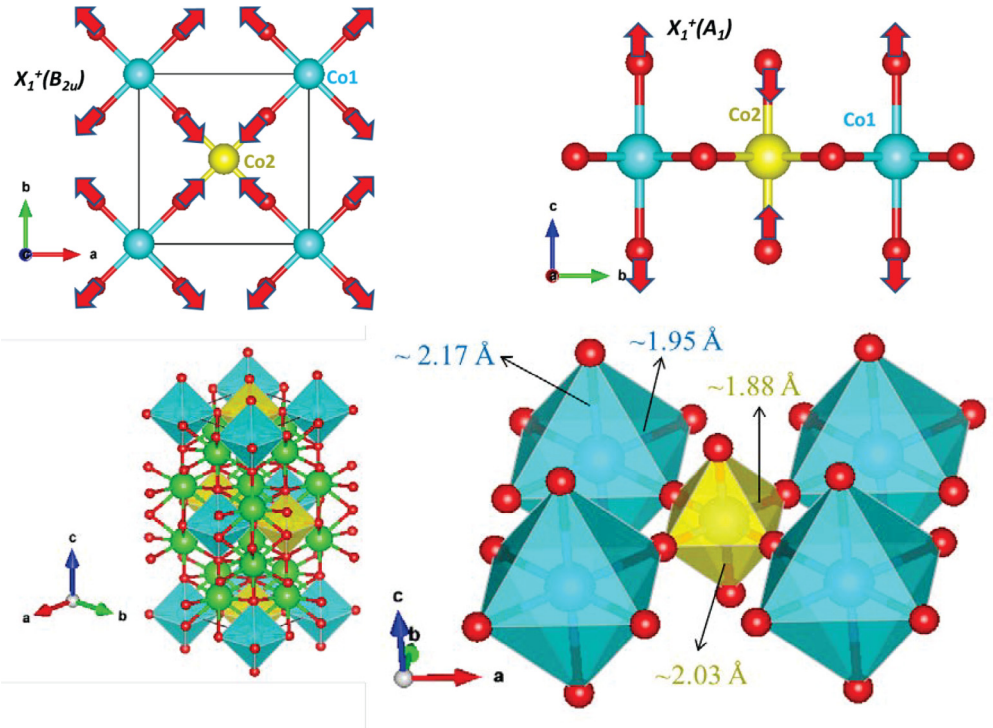

FIG. 10. Top: Atomic shifts for the equatorial (left) and apical (right) oxygen atoms associated to the condensation of the modes indicated in each figure. Bottom: Crystal structure of $La_{2-x}A_xCoO_{4\pm\delta}$ samples (A = Ca, Sr) in the orthorhombic $A2mm$ symmetry (left) and a picture with the top monolayer (right) composed by $Co2O_6$ (small octahedron, yellow online) and $Co1O_6$ (big octahedra, blue online). Big spheres stand for Co1 (blue online), Co2 (yellow online), and La/A (green online) atoms whereas oxygen is represented by small spheres (red online). Representative Co-O bond lengths in the $A2mm$ ordered phase are indicated for each type of octahedron. The picture does not follow the real scale and distortions of the octahedra have been exaggerated to facilitate their interpretation.

Co^{3+} in an octahedral oxygen environment [42] is about 2.6 eV, this means that the charge segregation between Co1 and Co2 sites is about 0.6 ± 0.1 electron. The unpolarized XANES spectra of Co1 and Co2 sites compare quite well with those of $La_2CoO_{4.2}$ and $LaSrCoO_{3.99}$, respectively in what regards the energy position of the absorption edge, which results in a charge difference between the nominal average Co oxidation states of 0.42 ± 0.1 electron, as reported in the Experimental section.

Due to the relationship between the valence state and the local structure, we have carried out theoretical simulations of the different resonant reflections in $La_{1.5}Ca_{0.5}CoO_{4.02}$ making use of the FDMNES code [35] to determine the associate geometrical distortions of the two different Co sites. This program calculates from first principles the x-ray-absorption coefficient and the anomalous atomic scattering factor tensor as a function of the photon energy for the different crystallographic sites. The intensity of resonant reflections is then calculated using these atomic scattering factors for a finite cluster of atoms surrounding the absorbing one. The starting structural model for all the simulations was the orthorhombic $A2mm$ structure but with lattice parameters and fractional coordinates correspondent to the undistorted tetragonal structure obtained by synchrotron x-ray diffraction for the $La_{1.5}Ca_{0.5}CoO_{4.02}$ sample. Then, only displacements of the oxygen atoms in the $A2mm$ unit cell have been considered in the simulations whereas La-Ca and Co positions have been kept. However, the code is not implemented to calculate the scattering from a random atomic distribution as present in our sample, i.e., La and Ca atoms occupy the same crystallographic site. To overcome this problem, we have carried out the theoretical simulations of the atomic scattering factor tensors for clusters with either only La or only Cd atoms since the atomic number of cadmium corresponds to three times the one of La plus one time that of Ca. The best result is obtained using cadmium as shown in Fig. 9 and the refined fractional coordinates of the oxygen atoms in the ab plane are O1 ($x = 0.2559$; $y = 0.254$) and O2 ($x = 0.7441$; $y = 0.746$), which corresponds to a distortion of $\Delta x = 0.0319$ Å and $\Delta y = 0.0216$ Å, being the expansion and compression in the ab plane, 0.0385 Å. For the apical oxygens, we found O3 ($z = 0.1755$) and O4 ($z = 0.164$), which corresponds to a distortion of $\Delta z = 0.068$ Å. Figure 10 outlines the local structure of the two nonequivalent CoO_6 octahedra including the values of the Co-O bond lengths as extracted from this paper. It is clear that both CoO_6 are distorted with the apical Co-O distances longer than equatorial Co-O ones. The oxygen shifts lead to two kinds of CoO_6 octahedra: one compressed (Co2) and the other expanded (Co1). The correspondent FDMNES calculated XANES spectra for these two kinds of octahedra show a chemical shift of about 1.3 eV, which means a charge segregation of about 0.5 ± 0.1 electron. This disproportionation coincides with that estimated previously by the semiempirical method within the uncertainty.

The previous atomic shifts can be understood in the frame of a symmetry-mode analysis considering the structural transition

from the tetragonal $I4/mmm$ phase to the orthorhombic $A2mm$. In this transition, there are two active modes belonging to the same irreducible representation (Irrep) X_1^+ that reproduce the above-mentioned oxygen movements. As can be seen in Fig. 10, the $X_1^+(B_{2u})$ mode acts on the equatorial oxygen atoms of CoO_6 octahedra producing a stretching around the Co1 and a compression around Co2. Moreover, the mode $X_1^+(A_1)$ acts on the apical oxygen atoms leading to an elongation of Co1-O bonds coupled to a shortening of the Co2-O ones.

We have measured high-resolution synchrotron powder XRD patterns at room temperature on several $La_{1-x}Ca_xCoO_{4\pm\delta}$ samples and no superstructure peaks arising from the condensation of the previous modes were detected. Therefore, we have performed simulations of the expected patterns with different distortion degrees and small superstructure peaks are only noticeable from the experimental background for oxygen shifts between 70 and 100% larger than the experimentally observed. It is noteworthy that condensation of X_1^+ modes alone does not lead to the $A2mm$ symmetry but to the $Ammm$ one. As we do not need further distortions to account for the RXS measurements, our paper does not give any evidence for a polar structure in the so-called CO arrangement of this family of cobaltites.

IV. CONCLUSIONS

We have presented an extensive resonant x-ray scattering investigation of the charge superstructures in the layered cobalt oxides $La_{2-x}Ca_xCoO_{4\pm\delta}$ ($x = 0.4$, 0.5, 0.6, and 0.7) and $La_{1.5}Sr_{0.5}CoO_{3.99}$. All the studied samples show the same checkerboard pattern of ordering of two different Co sites giving rise to $(h/2, h/2, l)$-type superstructure reflections and the lack of any local anisotropy ordering with the periodicity given by $(h/4, h/4, l)$-type reflections. To analyze the resonant x-ray data, a semiempirical method has been shown. The real part of the resonant structure factor can be obtained by the subtraction of the experimental RXS spectra of two resonant $(h/2, h/2, l)$-type reflections with identical resonant structure factor that either adds to or subtracts from the Thomson term depending on the h index. This simple approach in combination with conventional XANES spectra has allowed us to obtain the site-resolved XANES spectra (or the imaginary part of the resonant atomic scattering factors) for the two nonequivalent Co sites, which results in a charge disproportionation of about 0.6 electron in the ordered phases. From the comparison with the experimental XANES spectra of the nominal La_2CoO_4 and $LaSrCoO_4$ samples, the energy position of the absorption edge for each of these two distinct Co atoms is close to that of the nominal La_2CoO_4 and $LaSrCoO_4$ reference samples, which at first justifies the analysis made by Horigane *et al.* in a previous RXS study [29]. However, we have found that the oxygen content of the reference samples is $La_2CoO_{4.2}$ and $LaSrCoO_{3.91}$ so the correspondent valence states are $Co^{2.4+}$ and $Co^{2.82+}$. Finally, since the valence state is intimately related to the local structure [43], the simulation of the experimental RXS spectra by FDMNES [35] shows that the checkerboard ordering is formed by alternating expanded and compressed CoO_6 octahedra, the average charge disproportionation on these sites being about 0.5 electron. The appearing of these local distortions comes from the condensation of two soft modes —$X_1^+(B_{2u})$ and $X_1^+(A_1)$— acting on the equatorial and apical oxygen atoms, respectively.

Therefore, the half-doped layered transition-metal oxides $RE_{1.5}A_{0.5}TMO_4$ (RE = rare earth; A = Ca, Sr; and TM = Mn, Ni, Co) show a common checkerboard ordering of two nonequivalent TM atoms associated to two distinct valence states. Despite this same pattern of ordering, marked differences are found in the magnitude of the charge disproportionation. Compared to $La_{1.5}Sr_{0.5}MnO_4$, where a maximum charge disproportionation of 0.15 electron was determined [13], either the magnitude of the charge disproportionation or the compression and expansion of the oxygen octahedra is relatively high (∼0.5 electron) in the layered cobalt oxides. Based on the fact that CO transitions are driven by concomitant structural transitions, the reason for this may come from the fact that CO appears at much higher temperatures (T_{CO} well above room temperature) in these layered cobalt oxides than in the layered manganites ($T_{CO} \sim 230$ K). Generally, the magnitude of a distortion is correlated with the temperature in which the ordered phase is stabilized because local distortions compete with the thermal motion. In this way, larger distortions can be frozen at higher temperatures.

Clear differences are also observed in the type of ordering for compositions far from the half doping depending on the TM atom. In the layered manganites the checkerboard ordering is maintained for doping $x < 0.5$ and an incommensurate sinusoidal modulation is observed for $x > 0.5$ whereas the $La_{2-x}A_xNiO_4$ and $La_{2-x}A_xCoO_{4\pm\delta}$ series seem to maintain the checkerboard ordering of only two sites for all compositions with $x \neq 0.5$. The reason is that the hole doping does not follow the Ca content in the $La_{2-x}A_xCoO_{4\pm\delta}$ series. As it is shown in the Experimental section, the average Co valence state is modulated by the oxygen stoichiometry in such a way that all the samples from $x = 0.4$ up to 0.7 have very similar Co valence state close to the $Co^{+2.5}$. Moreover, manganites also show a local anisotropy ordering (so-called orbital ordering) due to the presence of a Jahn-Teller distortion of one of the two Mn sites. This kind of distortion is absent in the present family of cobaltites so that $(h/4, h/4, l)$-type reflections are not observed.

In conclusion, our paper demonstrates that the charge-ordered phases in the $La_{2-x}Ca_xCoO_{4\pm\delta}$ ($0.4 < x < 0.7$) series correspond to a checkerboard ordering formed by two types of compressed and expanded CoO_6 octahedra, with an average associated charge disproportionation of about 0.5 ± 0.1 electron. For the $La_{1.5}Sr_{0.5}CoO_{3.99}$ sample, the same type of order and charge disproportionation can be inferred but the ordering only extends coherently for few crystallographic cells. Finally, we believe that the empirical method shown in this paper is particularly useful to resolve the indetermination coming from the relative magnitude between the resonant structure factor and the Thomson term in the analysis of RXS data.

ACKNOWLEDGMENTS

The authors would like to acknowledge the ESRF for granting beam time, and BM02 and BM23 staff for technical assistance. We would also like to thank the

ALBA synchrotron for granting beam time to perform the high-resolution XRD measurements in collaboration with the BL04-MSPD beamline staff. Authors would like to acknowledge the use of *Servicio General de Apoyo a la Investigación—SAI, Universidad de Zaragoza*. For financial support, we thank the Spanish Ministerio de Economía y Competitividad Project No. MAT2015-68760-C2-1-P and Diputación General de Aragón Project No. E69.

[1] G. R. Stewart, Adv. Phys. **66**, 75 (2017).
[2] M. Imada, A. Fujimori, and Y. Tokura, Rev. Mod. Phys. **70**, 1039 (1998).
[3] S. Lafuerza, J. García, G. Subías, J. Blasco, and P. Glatzel, Phys. Rev. B **93**, 205108 (2016).
[4] M. Fiebig, T. Lottermoser, D. Meier, and M. Trassin, Nat. Rev. Mater. **1**, 16046 (2016).
[5] Y. Moritomo, Y. Tomioka, A. Asamitsu, Y. Tokura, and Y. Matsui, Phys. Rev. B **51**, 3297 (1995).
[6] J. M. Tranquada, B. J. Sternleib, J. D. Axe, Y. Nakamura, and S. Uchida, Nature (London) **375**, 561 (1995).
[7] C. H. Chen, S.-W. Cheong, and A. S. Cooper, Phys. Rev. Lett. **71**, 2461 (1993).
[8] J. M. Tranquada, D. J. Buttrey, V. Sachan, and J. E. Lorenzo, Phys. Rev. Lett. **73**, 1003 (1994).
[9] K. Yamada, T. Omata, K. Nakajima, Y. Endoh, and S. Hosoya, Physica C **221**, 355 (1994).
[10] M. Cwik, M. Benomar, T. Finger, Y. Sidis, D. Senff, M. Reuther, T. Lorenz, and M. Braden, Phys. Rev. Lett. **102**, 057201 (2009).
[11] Y. Murakami, H. Kawada, H. Kawata, M. Tanaka, T. Arima, Y. Moritomo, and Y. Tokura, Phys. Rev. Lett. **80**, 1932 (1998).
[12] B. J. Sternlieb, J. P. Hill, U. C. Wildgruber, G. M. Luke, B. Nachumi, Y. Moritomo, and Y. Tokura, Phys. Rev. Lett. **76**, 2169 (1996).
[13] J. Herrero-Martín, J. Blasco, J. García, G. Subías, and C. Mazzoli, Phys. Rev. B **83**, 184101 (2011).
[14] P. Mahadevan, K. Terakura, and D. D. Sarma, Phys. Rev. Lett. **87**, 066404 (2001).
[15] J. Wang, W. Zhang, and D. Y. Xing, J. Phys.: Condens. Matter **14**, 4659 (2002).
[16] R. Kajimoto, K. Ishizaka, H. Yoshizawa, and Y. Tokura, Phys. Rev. B **67**, 014511 (2003).
[17] J. Okamoto, H. Nakao, Y. Yamasaki, H. Wadati, A. Tanaka, M. Kubota, K. Horigane, Y. Murakami, and K. Yamada, J. Phys. Soc. Jpn. **83**, 044705 (2014).
[18] C. F. Chang, Z. Hu, Hua Wu, T. Burnus, N. Hollmann, M. Benomar, T. Lorenz, A. Tanaka, H.-J. Lin, H. H. Hsieh, C. T. Chen, and L. H. Tjeng, Phys. Rev. Lett. **102**, 116401 (2009).
[19] P. G. Radaelli and S.-W. Cheong, Phys. Rev. B **66**, 094408 (2002).
[20] K. Knízek, P. Novák, and Z. Jirak, Phys. Rev. B **71**, 054420 (2005).
[21] J. L. García-Muñoz, C. Frontera, A. J. Barón-González, S. Valencia, J. Blasco, R. Feyerherm, E. Dudzik, R. Abrudan, and F. Radu, Phys. Rev. B **84**, 045105 (2011).
[22] N. Hollmann, M. W. Haverkort, M. Benomar, M. Cwik, M. Braden, and T. Lorenz, Phys. Rev. B **83**, 174435 (2011).
[23] Y. Moritomo, K. Higashi, K. Matsuda, and A. Nakamura, Phys. Rev. B **55**, R14725 (1997).
[24] N. Sakiyama, I. A. Zaliznyak, S.-H. Lee, Y. Mitsui, and H. Yoshizawa, Phys. Rev. B **78**, 180406 (2008).
[25] K. Horigane, H. Hiraka, T. Uchida, K. Yamada, and J. Akimitsu, J. Phys. Soc. Jpn. **76**, 114715 (2007).
[26] J. García, J. Herrero-Martín, G. Subías, J. Blasco, J. S. Andreu, and M. C. Sánchez, Phys. Rev. Lett. **109**, 107202 (2012).
[27] G. Subías, J. García, J. Herrero-Martín, J. Blasco, and M. C. Sánchez, J. Phys. Conf. Series **519**, 012008 (2014); J. García, J. Herrero-Martín, G. Subías, J. Blasco, and M. C. Sánchez, *ibid.* **430**, 012107 (2013).
[28] J. Blasco, J. García, G. Subías, H. Renevier, M. Stingaciu, K. Conder, and J. Herrero-Martín, Phys. Rev. B **78**, 054123 (2008).
[29] K. Horigane, H. Nakao, Y. Kousaka, T. Murata, Y. Noda, Y. Murakami, and J. Akimitsu, J. Phys. Soc. Jpn. **77**, 044601 (2008).
[30] J. Blasco, M. C. Sánchez, J. García, J. Stankiewicz, and J. Herrero-Martín, J. Cryst. Growth **310**, 3247 (2008).
[31] J. Rodríguez-Carvajal, Physica B **192**, 55 (1993).
[32] M. Karppinen, M. Matvejeff, K. Salomäki, and H. Yamauchi, J. Mater. Chem. **12**, 1761 (2002).
[33] F. Fauth, I. Peral, C. Popescu, and M. Knapp, Powder Diffr. **28**, S360 (2013).
[34] J. L. Ferrer, J. P. Simon, J. F. Bérar, B. Caillot, E. Fanchon, O. Kaïkati, S. Arnaud, M. Guidotti, M. Pirocchi, and M. Roth, J. Synchr. Rad. **5**, 1346 (1998).
[35] Y. Joly, Phys. Rev. B **63**, 125120 (2001).
[36] O. Mathon, A. Betheva, J. Borrel, D. Bugnazet, S. Gatla, R. Hino, I. Kantor, T. Mairs, M. Muñoz, S. Pasternak, F. Perrin, and S. Pascarelli, J. Synchr. Rad. **22**, 1548 (2015).
[37] S. Lafuerza, G. Subías, J. García, J. Blasco, G. Nisbet, K. Conder, and E. Pomjakushina, Phys. Rev. B **90**, 085130 (2014).
[38] M. Blume, J. Appl. Phys. **57**, 3615 (1985).
[39] H. Templeton and L. K. Templeton, Phys. Rev. B **49**, 14850 (1994).
[40] E. Dmitrienko, K. Ishida, A. Kirfel, and E. N. Ovchinnikova, Acta Crystallogr. Sect. A **61**, 481 (2005).
[41] A. Aguadero, J. A. Alonso, and L. Daza, Z. Naturforsch. **63b**, 615 (2008).
[42] V. Cuartero, S. Lafuerza, M. Rovezzi, J. García, J. Blasco, G. Subías, and E. Jiménez, Phys. Rev. B **94**, 155117 (2016).
[43] J. García, G. Subías, V. Cuartero, and J. Herrero-Martín, J. Synchr. Rad. **17**, 386 (2010).